PAPER V

Parametric study of the time-averaged gas–solid drag force in circulating fluidized bed conditions

Powder Technology 257 (2014a) 20–29.

Powder Technology 257 (2014) 20–29

Contents lists available at ScienceDirect

Powder Technology

journal homepage: www.elsevier.com/locate/powtec

Parametric study of the time-averaged gas–solid drag force in circulating fluidized bed conditions

Sirpa Kallio *, Juho Peltola, Timo Niemi

VTT Technical Research Centre of Finland, P.O. Box 1000, FI-02044 VTT, Finland

ARTICLE INFO

Article history:
Received 7 October 2013
Received in revised form 19 December 2013
Accepted 7 February 2014
Available online 14 February 2014

Keywords:
Drag force
Circulating fluidized bed
Time-averaging
Computational fluid dynamics

ABSTRACT

Steady state modeling based on time-averaged transport equations is a computationally efficient method for CFD simulation of large industrial-scale circulating fluidized beds. The feasible alternative for steady state modeling is to carry out transient simulations in a coarse mesh, which would require mesh resolution dependent closure laws and lead to long simulations in order to characterize the average process behavior. These closures could be avoided by simulations with adequate spatial and temporal resolutions, but the required computational effort renders such simulations unfeasible in industrial scale applications in near future. Equation closures for steady state modeling can be developed by time-averaging results from transient simulations. One of the largest terms to be modeled is the time-averaged drag force. In the present work, parameters that need to be accounted for in a model for the time-averaged drag force were studied by analyzing time-averaged results from a number of transient 2D simulations carried out with fairly fine spatial resolution. The analysis was limited to Geldart B particles. In the literature, the solid volume fraction, distance to the wall and the gas–solid slip velocity have been included as parameters in drag correction functions developed for transient coarse-mesh simulations. In the present work, the same parameters are found to have significant effects on the time-averaged gas–solid drag force. Additionally, solid density, particle size and gas phase laminar viscosity are shown to have significant effects on the average drag force. Thus process conditions, which significantly vary inside a CFB, need to be accounted for in the model.

1. Introduction

The flow patterns in a circulating fluidized bed (CFB) are characterized by large spatial and temporal fluctuations in solid concentration as well as in gas and solid velocities. Length scales of these variations can be very small, down to a few particle diameters, which constitutes a difficult challenge for computational fluid dynamic (CFD) simulation of industrial scale CFBs utilized in energy production and conversion processes. Similar computational mesh related spatial resolution challenges are encountered both with Eulerian–Eulerian two-fluid models and with the multi-phase particle-in-cell methods [1]. Resolving the smallest flow structures would require a very fine mesh that would be computationally unfeasible for simulation of typical industrial scale processes. As a result, coarser meshes that filter out the fine sub-grid scale flow structures are commonly used. To account for the filtered information, corrections or sub-grid scale models for the terms in the transport equations should be applied. Such closure models have been proposed in the literature for different terms in the gas and solid phase momentum equations on the basis of theoretical considerations and analysis of results from transient simulations of fairly small geometries with high spatial resolution. As the filtering scale depends on the resolution of the simulation, these closure models should have the resolution as a parameter which complicates derivation of the closure laws. No general closures that would cover all typical conditions in circulating fluidized beds and all terms in the equations have yet been proposed.

To avoid mesh dependence in the closures and to speed up the simulations, steady state modeling has been suggested as an alternative for the transient simulations [2,3]. Transient coarse mesh simulations filter out spatial fluctuations smaller than the mesh spacing and temporal fluctuations shorter than the time step. Steady-state simulation models are derived by time-averaging the transient equations, which filters out all temporal variations in the flow properties. Closures need to be developed to account for the effects of the filtered variations. These closures are of a similar character as the sub-grid closures required for transient coarse mesh simulations. In both cases, the closures describe clustering of particles and fluctuations in flow properties. A closure for a very coarse mesh should approach the closure for a time-averaged equation, since a volume average over a distance longer than the longest length-scales of the fluctuations should produce the same result as a time

* Corresponding author. Tel.: +358 20 7224015.
E-mail address: sirpa.kallio@vtt.fi (S. Kallio).

http://dx.doi.org/10.1016/j.powtec.2014.02.022
0032-5910/

average in a single point, when the statistical characteristics over the averaging space and time frame are the same. That would be the case if there would be no spatial gradients in the time-averaged flow field. Although this condition is never exactly met, the gradients in the time-averaged volume fraction and velocities are often small compared to the fluctuations, for example in the center of a large CFB riser.

To evaluate the need for equation closures, a study of the terms in the time-averaged momentum equations in CFB conditions was carried out by Kallio et al. [4]. One of the largest terms in the momentum equations was the gas–solid drag force, for which several closures have been proposed to describe the effects of clustering of particles. Closures can be derived on experimental basis like what was done by Kallio et al. [5] who applied a drag law that was based on the empirical equations suggested by Matsen [6] for bed expansion in CFB and BFB conditions and on the Ergun [7] equation at the packing limit. In recent years, instead of using empirical correlations as basis, it has been more common to develop models based on transient simulations in fine meshes.

Agrawal et al. [8], Andrews et al. [9], and Igci et al. [10,11] developed closures for the average drag and stress terms through 2D simulations in small domains with periodic boundary conditions and, by volume-averaging the results, they derived closures for the sub-grid scales. In Igci and Sundaresan [12] and Igci et al. [13], wall effects were included in the analysis of a case of Geldart A particles and in the closures that were derived by volume-averaging 2D transient simulation results for the drag force and the normal and shear stresses of the solid phase. Milioli et al. [14] further developed the closures by including the slip velocity between the phases in the equations. Shah et al. [15] studied wall effects on the gas–solid drag force in a case of Geldart B particles through volume-averaging 2D transient simulation results for a small CFB. Zhang and VanderHeyden [16] discussed the effects of mesh spacing on Reynolds stresses and the drag force. In Zhang and VanderHeyden [17], an added-mass force closure was suggested for the correlation between fluctuations of the pressure gradient of the continuous phase and fluctuations of solid volume fraction. De Wilde [18] analyzed the same term from simulations and accounted also for the average drag force in the derivation of new closure models that were applied in De Wilde et al. [19] for steady state simulation of a riser. In addition to models based on measurement data and transient simulation results, closures for the gas–solid drag force have been suggested on the basis of theoretical analysis of clustering flow in dense gas–solid suspensions [20,21]. Common to all the suggested sub-grid and steady-state drag models is that the predicted drag force is reduced from what the homogeneous flow drag correlations would predict in the same flow conditions.

The models presented in the literature often take into account only a small number of factors that can affect the magnitude of fluctuations in flow properties. To improve our understanding of the requirements for a comprehensive filtered drag law, the present study analyzes the effects of material properties on the average drag force applicable to steady state modeling. In addition, the effects of process conditions on the required drag closures are evaluated. The analysis is based on time-averaging the results from transient Eulerian–Eulerian simulations of circulating fluidized beds of Geldart B particles. Since 3D simulations are very time consuming, development of sub-grid closure laws has commonly been carried out by averaging results from 2D simulations. For the same reason, this parametric study is carried out in 2D. Although the observed quantitative effects of the studied parameters cannot be applied to 3D simulations with high accuracy, some implications for further 3D studies and closure development can be derived, since the parameters required for drag correction in 2D should be significant also in 3D geometries. Still, as long as a similar dataset from 3D simulations is not available, the data collected in the present study can be used to derive models for the time-averaged drag force. Furthermore, the results of the present study provide an indication which parameters should be included in the drag correction functions applicable to coarse mesh simulations.

2. Methodology

2.1. Transient simulations

A large number of 2D simulations were carried out for analysis of the required closures for the time-averaged momentum equations. A selection of the simulations with varying gas viscosities, gas densities, solid densities, particle sizes, riser size and mesh spacings was chosen for the present analysis. The geometry is a simple riser with straight walls. A uniform gas inflow is introduced at the bottom and gas and solids exit the riser through the top edge of the simulated domain. Solids that leave the riser are fed back through a return channel located at 0.6–0.7 m height.

The simulations analyzed are listed in Table 1. Although gas density and viscosity in most industrial applications are strongly coupled, here their values were changed independently to separate their individual effects. Thus some of the simulations don't necessarily represent typical CFB conditions as used today.

The numerical simulations were carried out with the commercial code ANSYS Fluent v.14 [22]. The simulations were based on the Eulerian–Eulerian multiphase approach with the kinetic theory of granular flow (KTGF) models. In this study, models available in Fluent v.14 were used and they are listed in Table 2 with references to the corresponding authors.

For the drag term the standard Gidaspow [23] model based on the Ergun [7] and Wen–Yu [24] drag laws was used. For the momentum second order discretization was applied and for the volume fraction equation the QUICK scheme was applied. The time step was 0.001 s for the 12.5 mm and 25 mm meshes and 0.0005 s for the 6.25 mm mesh. For each case, approximately 5 s was simulated before starting to calculate the average values and at least a further 120 s of flow time was simulated to compute the averages. This presented a reasonable compromise between simulation time and accuracy of the average values. Comparisons with measurements have been made earlier for some simulations with the same models in a 0.4 m wide geometry [25]. The measurement and simulation results were in good qualitative agreement and even quantitatively the results were reasonably good considering that the simulations were carried out in 2D. Thus the chosen approach should be sufficiently accurate for the present study.

To allow simulation of a large number of cases in a reasonably short time, most simulations in this work were carried out in a coarse mesh with 12–25 mm spacing. To study effects of the mesh spacing, one simulation was done in a finer 6.3 mm mesh. At the same time, also the time step was halved, i.e., reduced from 0.001 s to 0.0005 s. Fig. 1 shows a comparison of the obtained time-averaged solid volume fraction fields in Cases 1, 3 and 2, where the mesh spacing was 6.3 mm, 12.5 mm and 25 mm, respectively. No significant qualitative change in the solid distribution can be observed. The majority of the simulations analyzed in the present work were carried out in a 2D mesh with 12.5 mm mesh spacing. Although the quantitative results slightly change when the mesh is coarsened, the qualitative results don't show any significant sensitivity to mesh spacing and time step and thus the chosen meshes were considered sufficient for this qualitative parametric study. Some simulations were also carried out in a 50 mm mesh, which produced significantly altered flow patterns. Consequently, simulations with such coarse meshes were omitted from the analysis.

2.2. Time-averaging of the transient simulation results

Time-averaged equations can be developed by averaging the transient equations over time. The instantaneous values are written as a sum of the time-average and a fluctuation: $\phi = \overline{\phi} + \phi'$. Favre averaging is applied on velocities: $U_{q,i} = \overline{\alpha_q u_{q,i}}/\overline{\alpha_q}$, $u_{q,i} = U_{q,i} + u''_{q,i}$. The time-

Table 1
Analyzed cases. Parameters: gas superficial velocity U_0, gas viscosity μ_g, gas density ρ_g, solid density ρ_s, particle diameter d_p, mesh spacing Δx_{mesh}, riser width w, riser height h, terminal velocity v_t, particle Reynolds number at terminal velocity Re_t, average solid volume fraction $\overline{\alpha_s}$, and static pressure at the bottom p_{bot}.

Case	U_0	μ_g	ρ_g	ρ_s	d_p	Δx_{mesh}	w	h	v_t	Re_t	$\overline{\alpha_s}$	p_{bot}
	m/s	kg/m s	kg/m^3	kg/m^3	mm	mm	m	m	m/s	–	%	kPa
1	3.5	1.79E−05	1.225	2480	0.385	6.3	0.4	3	2.85	75	5.38	2.70
2	3.5	1.79E−05	1.225	2480	0.385	25	0.4	3	2.85	75	5.39	2.72
3	3.5	1.79E−05	1.225	2480	0.385	12.5	0.4	3	2.85	75	5.39	2.96
4	3.5	1.79E−05	1.225	2000	0.385	12.5	0.4	3	2.47	65	5.39	2.81
5	3.5	1.79E−05	1.5925	2480	0.385	12.5	0.4	3	2.61	89	5.40	4.24
6	3.5	1.79E−05	0.8575	2480	0.385	12.5	0.4	3	3.22	59	5.39	3.28
7	3.5	2.79E−05	1.225	2480	0.385	12.5	0.4	3	2.45	41	5.39	6.46
8	3.5	7.90E−06	1.225	2480	0.385	12.5	0.4	3	3.61	216	5.39	3.67
9	2.75	4.45E−05	0.3105	2480	0.2555	12.5	0.4	3	1.53	2.7	6.80	4.49
10	2.75	4.45E−05	0.3105	2480	0.2555	12.5	1	7	1.53	2.7	2.97	3.55
11	2.75	4.45E−05	0.3105	2480	0.2555	12.5	3	14	1.53	2.7	1.49	5.04
12	2.75	4.45E−05	0.3105	2480	0.2555	12.5	3	14	1.53	2.7	4.34	12.4
13	2	4.45E−05	0.3105	2480	0.2555	12.5	3	14	1.53	2.7	1.49	4.93
14	5	4.45E−05	0.3105	2480	0.2555	12.5	3	14	1.53	2.7	1.49	5.30
15	5	4.45E−05	0.3105	2480	0.44	12.5	3	14	3.37	10	1.48	4.27
16	5	4.45E−05	0.3105	2480	0.15	12.5	3	14	0.62	0.64	1.48	4.68
17	8	4.45E−05	0.3105	2480	0.2555	12.5	3	14	1.53	2.7	1.48	5.10

averaged continuity and momentum equations for phase q (changes in ρ_{qm} assumed small) can be written as follows [2]:

$$\frac{\partial \overline{\alpha}_q \rho_{qm}}{\partial t} + \frac{\partial \overline{\alpha}_q \rho_{qm} U_{q,k}}{\partial x_k} = 0 \tag{1}$$

$$\begin{aligned}\frac{\partial \overline{\alpha}_q \rho_{qm} U_{q,i}}{\partial t} + \frac{\partial \overline{\alpha}_q \rho_{qm} U_{q,k} U_{q,i}}{\partial x_k} &= \overline{\alpha}_q \rho_{qm} g_i - \overline{\alpha}_q \frac{\partial \overline{p}}{\partial x_i} - \overline{\alpha_q'} \frac{\partial p'}{\partial x_i} + \frac{\partial \overline{\alpha_q \tau_{q,ik}}}{\partial x_k} \\ &+ \frac{\partial \overline{\alpha_q \tau^M_{q,ik}}}{\partial x_k} + (-1)^{(\delta_{qs}+1)} K_{gs}\left(u_{g,i} - u_{s,i}\right) \\ &- \frac{\partial \overline{p}_q}{\partial x_i}\delta_{qs} - \frac{\partial \rho_{qm} \overline{\alpha_q u''_{q,k} u''_{q,i}}}{\partial x_k}.\end{aligned} \tag{2}$$

Here ρ is the density, α volume fraction, p pressure, p_s solid pressure, g gravitational acceleration, K inter-phase momentum transfer coefficient, δ_{gs} Kronecker delta, τ laminar stress, and τ^M local-scale turbulent stress. The time average of a variable φ is denoted by $\overline{\varphi}$ and the fluctuation part by $\varphi' = \varphi - \overline{\varphi}$. In the equations above, u is the instantaneous velocity, U_q is the Favre average or phase-weighted average velocity $U_q = \overline{\alpha_q u_q}/\overline{\alpha_q}$ and $u''_q = u_q - U_q$ is the velocity fluctuation. The gas phase is denoted by g and solid phase by s. The terms on the right hand side in Eq. (2) are the gravitation term, pressure term, pressure fluctuation term, laminar stress, turbulent stress, drag force, solid pressure term, and the Reynolds stress term. The gravitation and pressure terms can be calculated from the basic average flow properties but for the rest of the terms closure relations have to be developed.

In the present study we concentrate on the time-averaged drag force in the vertical (y) direction and utilize for the analysis the time-averaged velocity and volume fraction fields. A closure for the time-averaged drag force can be written in the form.

$$\overline{K_{gs}\left(u_{g,y} - u_{s,y}\right)} = C_{drag} K^*_{gs}\left(U_{g,y} - U_{s,y}\right) \tag{3}$$

where K^*_{gs} is the inter-phase momentum transfer coefficient calculated on the basis of the time-averaged velocities and volume fractions using a similar combination of Wen and Yu [24] and Ergun [7] drag laws as in the transient simulations. However, instead of using Gidaspow's [23] drag law implemented in Fluent, a smoother transition between the drag laws, suggested by Niemi et al. [30], was used to calculate K^*_{gs}. In this model a linear transformation between the Ergun and Wen–Yu models occurs in a solid volume fraction range of 0.4–0.5, which is within the region recommended by Leboreiro et al. [31]. The coefficient C_{drag} in Eq. (3) is a drag correction coefficient, for which a correlation should be developed.

Table 2
The models and parameters used in the simulations.

Submodel or parameter	Model or value used
Granular viscosity	Syamlal et al. [26]
Granular bulk viscosity	Lun et al. [27]
Frictional viscosity	Schaeffer [28]
Granular conductivity	Syamlal et al. [26]
Solids pressure	Lun et al. [27]
Radial distribution	Ogawa et al. [29]
Angle of internal friction	30°
Frictional and packing limit	0.61 and 0.63, respectively
Turbulence model	Standard k − ε, dispersed
Wall boundary condition, gas	No slip
Wall boundary condition, solids	Partial slip, specularity coefficient 0.001

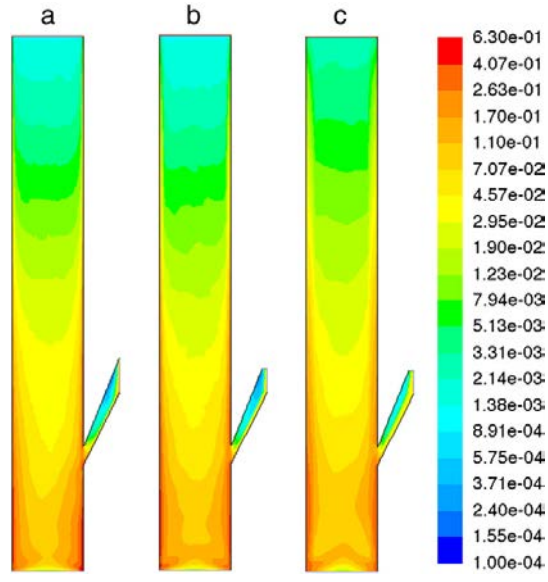

Fig. 1. Time-averaged solid volume fraction in simulations 1 (mesh spacing 6.3 mm), 3 (12.5 mm), and 2 (25 mm).

The value of C_{drag} in each point in the flow field can be calculated from Eq. (3) by time-averaging the drag force, solid volume fraction and gas and solid velocities over the simulation time of a transient simulation. This kind of data was collected for each of the cases listed in Table 1. Some filtering of the data was done at the data collection stage. For very low values of slip velocity, the computed C_{drag} can become unreasonably large due to stochastic nature of the data and finite averaging periods. C_{drag} values above 2.5 were removed from the data. The data for the solid return channel was also omitted from the analysis since the characteristics of the flow are there completely different. Similarly, exit region effects were avoided in the results by excluding the uppermost 20% of the simulated riser volume.

3. Results

3.1. Effect of solid volume fraction

Volume fraction of solid particles, α_s, is the most important parameter affecting the amount of correction that needs to be applied in clustering flow on the customary drag laws derived for homogeneous conditions. For that reason, the drag correction coefficient C_{drag} determined from the transient simulations is in the following plotted as a function α_s with other flow properties as parameters. In the comparisons, one parameter at a time has been varied in the simulations to allow easy comparison.

We start the analysis with Fig. 2 which shows the obtained values for C_{drag} as a function of α_s in all mesh points studied (the simulated domain except the return channel and riser exit region) in each of the cases listed in Table 1. In general we can observe a reduction of the average drag force from what is predicted by the homogeneous flow correlations. In the dilute end of the solid volume fraction scale at α_s values below 0.01 the relationship between C_{drag} and α_s is clear. In this region, C_{drag} for a set of conditions found in a single simulation could be expressed as a function of solid volume fraction only. In the dense regions the relationship is less clear and in an intermediate density range where α_s is of the order of 0.1 there is no correlation between C_{drag} and α_s. High solid concentrations are encountered in the wall layers and in the bottom bed where the flow patterns differ from the ones in the central part of the riser, which explains the different C_{drag} trends at high α_s.

In the dilute conditions, C_{drag} should approach unity since no drag correction needs to be applied for a single particle, i.e. for $\alpha_s \rightarrow 0$. Depending on fluidization conditions, the range of solid volume fractions strongly varies in the different cases in Fig. 2. In Case 10, where fluidization velocity is low, the suspension in the upper part of the riser is so dilute that the expected limit is reached. An interesting phenomenon seen in Fig. 2 is that in the dense suspension areas C_{drag} can also exceed 1. Exactly at packing limit it should go to unity, but in the CFB simulations of the present study the packing limit is not reached in the time-averaged data.

To analyze regional effects in Case 10, data from the riser bottom and wall regions is omitted in Fig. 3 in several steps. Fig. 3 reveals several interesting local effects. The C_{drag} values at around solid volume fraction 0.1 that show no clear correlation with solid content originate from the bottom section below 0.7 m elevation. Characteristic for this region is acceleration of solids from zero upward velocity at the bottom to a higher transport velocity. Fig. 3 also shows that the high values at low solid concentration appear in the near-wall region. The lowest values of C_{drag} originate from a region between 0.05 m and 0.1 m from the wall, which could be related to the location of the edge of the wall layer where both upward and downward movements of solids are common. In general, in the air entrance region the drag force seems to have a very different behavior compared to the rest of the riser and a separate analysis of this region might be necessary.

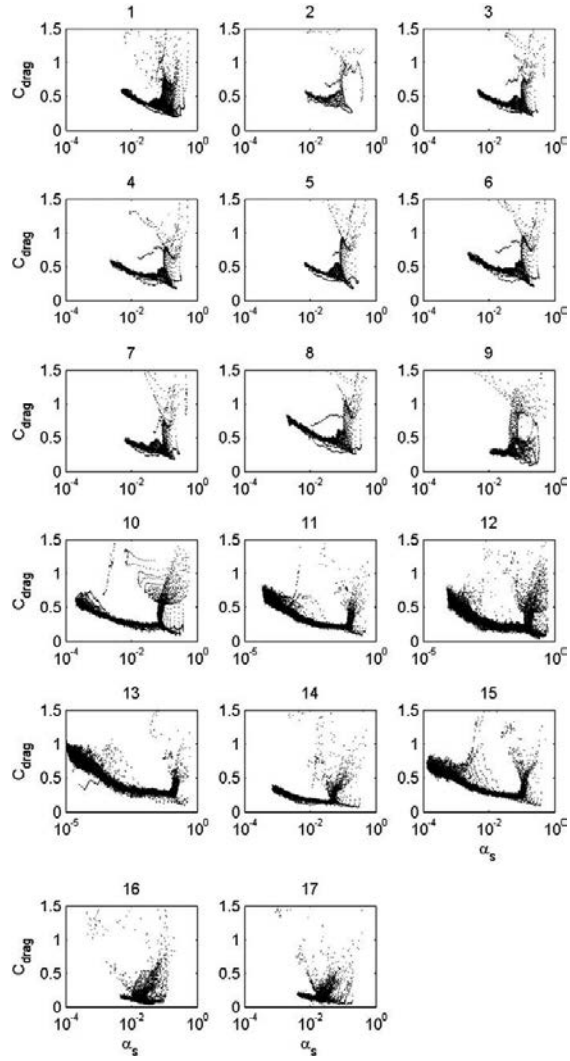

Fig. 2. The values of C_{drag} depicted as a function of α_s in all analyzed points in each of the 17 cases listed in Table 1.

3.2. Effect of mesh spacing

For practical reasons and to allow graphical presentation of the results, the amount of data plotted for comparisons of the different simulations was reduced by randomly picking points from the wall regions, from the bottom bed region and from the rest of the flow field, with different probabilities for the three regions to guarantee that all these regions are well represented in the plots.

Analysis of volume-averaged simulation results has shown [15,12] that in sub-grid closures for coarse mesh simulations, mesh size is an important parameter. It can be assumed that in the development of time-averaged models the mesh could play a role and hence the effect of the mesh that was used in the transient simulations needs to be evaluated.

Fig. 4 shows the effect of mesh spacing in Cases 1, 2 and 3. The same situation is simulated with three different mesh spacings, 6.3 mm,

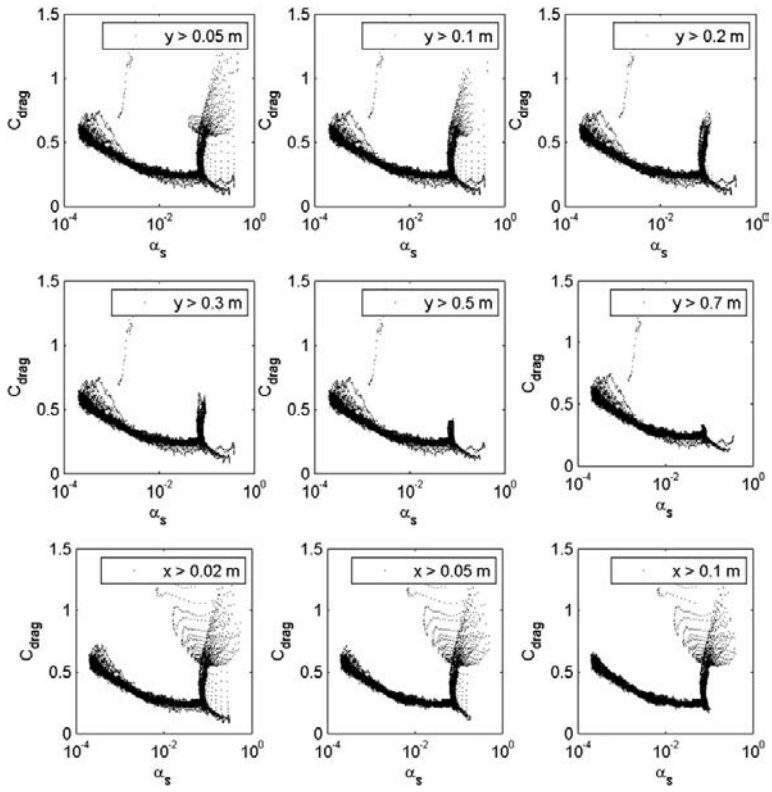

Fig. 3. The values of C_{drag} depicted as a function of α_s in limited regions in the riser in Case 10. In the figure, x is the lateral coordinate and y the vertical coordinate in the riser.

12.5 mm and 25 mm. The two finest meshes in Fig. 4 show practically the same results for C_{drag} whereas the 25 mm mesh has produced slightly higher values. Thus the 12.5 mm mesh can be considered accurate enough for the present analysis. Although Fig. 1 showed that there is a visible difference in the average volume fraction fields obtained with 6.3 mm and 12.5 mm meshes, the very small difference in the produced C_{drag} values indicates that the statistical properties of the fluctuations in the flow variables are fairly mesh independent at this mesh resolution,

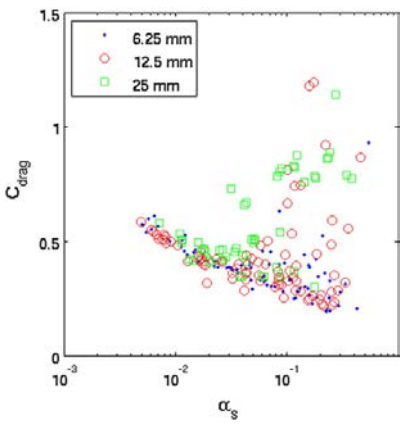

Fig. 4. Effect of mesh spacing on C_{drag} (Cases 1, 3, and 2, respectively, in Table 1).

which is a sufficient condition for accepting the coarser mesh for the analysis of the time-averaged drag force. This does not mean that all the finest flow structures are resolved by the simulation, but that the scales that have significant influence on the time-averaged drag force are captured. Results on C_{drag} obtained with the 25 mm mesh still show qualitatively similar trends and could probably also have been used for parametric studies. However, for derivation of closures, a finer mesh seems necessary.

3.3. Effects of process conditions

In CFBs the flow conditions can vary a great deal even when the temperature is constant and material properties are the same. Bed inventory and fluidization velocity change the voidage and velocity distributions in the process, which could affect solid clustering and hence also the drag correction required. In Fig. 5, results are shown for two simulations with the same gas and solid material properties and fluidization velocity but different solid inventory. The dependence of the drag correction values on the solid volume fraction is practically the same in the two simulations, which means that the bed mass need not to be separately accounted for. Fig. 6 illustrates that the fluidization velocity has no large effect either, although at the two lowest fluidization velocities higher C_{drag} is obtained. The differences can be due to changes in other parameters such as the average slip velocity. Fluidization velocity also affects the range of time-averaged volume fractions in the process. Largest range of solid concentrations is obtained at the small fluidization velocities. To obtain data for deriving a general drag correction function for the full range of flow conditions, simulations at several gas velocities can be necessary.

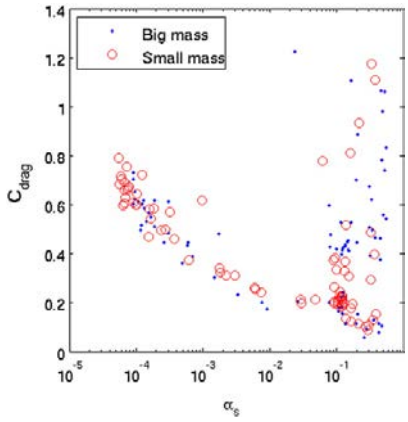

Fig. 5. Effect of bed mass on C_{drag} (Cases 12 and 11, respectively, in Table 1).

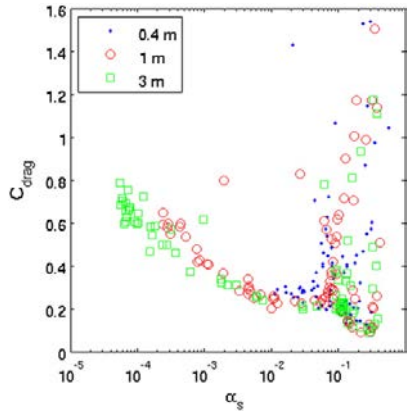

Fig. 7. Effect of riser width on C_{drag} (Cases 9, 10, and 11, respectively, in Table 1).

Riser width and height can also be expected to have an effect on the clustering tendency. Fig. 7 shows results from three simulations where the riser size has varied. A small effect on the drag function is visible in the figure. A bigger correction to the drag force, i.e. a smaller value of C_{drag} was obtained as the riser size was increased. The distance to the walls and the local slip velocity have been shown to have a significant effect in drag corrections required for coarse meshes [13,15] and these could also be behind the observed small effect on C_{drag}.

3.4. Effects of the distance to a wall and the slip velocity

Since in models for coarse meshes the lateral distance to the walls has been shown to be an important parameter, it can be assumed to have an effect also on the time-averaged drag force. In Fig. 8, the drag correction coefficient C_{drag} is plotted as a function of the distance to the wall for three different values of solid volume fraction, 0.001 (data in the range 0.0009–0.0011), 0.01 (0.009–0.011), and 0.1 (0.08–0.12). Wall distance seems to have a complicated effect. In Shah et al. [15] the correction coefficient in the sub-grid scale drag law, determined by volume averaging similar transient simulation results, diminished towards the wall. The same trend is seen in the time-averaged drag force in Fig. 8 in Case 14 for solid volume fraction 0.01, but in several other situations shown in Fig. 8 the trend is opposite. The flow pattern close to the wall can vary greatly depending on process conditions and the vertical position in the riser, which can be the reason behind the differences in the trends seen in Fig. 8.

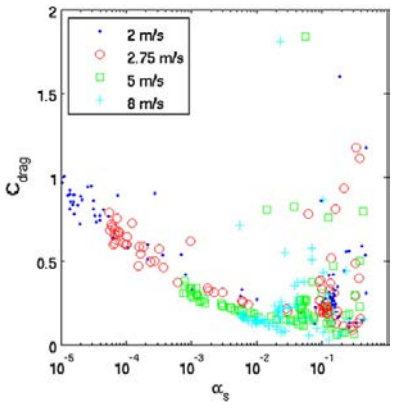

Fig. 6. Effect of fluidization velocity on C_{drag} (Cases 13, 11, 14, and 17, respectively, in Table 1).

Milioli et al. [14] reported that in addition to mesh spacing and the distance to the wall, also the slip velocity between gas and solid phases can play a significant role. The data from Cases 9, 10, 11, 12, 13, 14 and 17, with same material properties but different geometries and fluidization conditions is collected in Fig. 9 where the drag correction coefficient C_{drag} is shown at three solid volume fractions as a function of the lateral distance to a wall and as a function of the local vertical slip velocity component. A big scatter in the data is observed in both plots indicating that neither of these variables alone is capable of explaining the variation in C_{drag} at a fixed solid concentration.

To evaluate the combined effect of wall distance and slip velocity, data at a narrow range of wall distances were separated close to the wall (between 0.01 m and 0.03 m from the wall) and in the central region (distance to wall above 1.2 m). Fig. 10 shows the values of the drag correction coefficient at these two locations at the three studied solid volume fractions as a function of the slip velocity. It is evident that variations in the slip velocity can explain a significant fraction of the scatter visible in Fig. 9. An increase in the slip velocity leads to a lower C_{drag} value. In the central region some points at the two highest volume fractions don't fit the pattern. A closer look into these points showed that they are from the elements closest to the bottom plate. There the flow pattern will differ strongly from the rest of the riser and the drag correlation should perhaps be developed separately.

In the analyzed simulations, the no-slip boundary condition was used for the gas phase and partial slip condition with specularity coefficient 0.001 for the solid phase. Changing the value of the specularity coefficient could somewhat change the voidage and velocity profiles, especially close to the wall, and its effect on the behavior of C_{drag} as a function of the distance to the wall should also be checked in further studies. This was not done in the present work, where the same value as used in the validation study [25] was used in all simulations.

3.5. Effects of gas and solid properties

In the literature, no systematic study of the effects of phase properties on the drag correction coefficient has been presented. The data from the runs listed in Table 1 allows this kind of analysis. Initially in the present study a hypothesis was proposed that drag correction could be expressed as a function of dimensionless numbers such as the Reynolds number. In Fig. 11 results are plotted for Cases 5, 6, 7 and 8 with different Reynolds numbers that are calculated based on the particle terminal velocity. No simple clear trend as a function of the Reynolds number can be observed in these cases were gas density

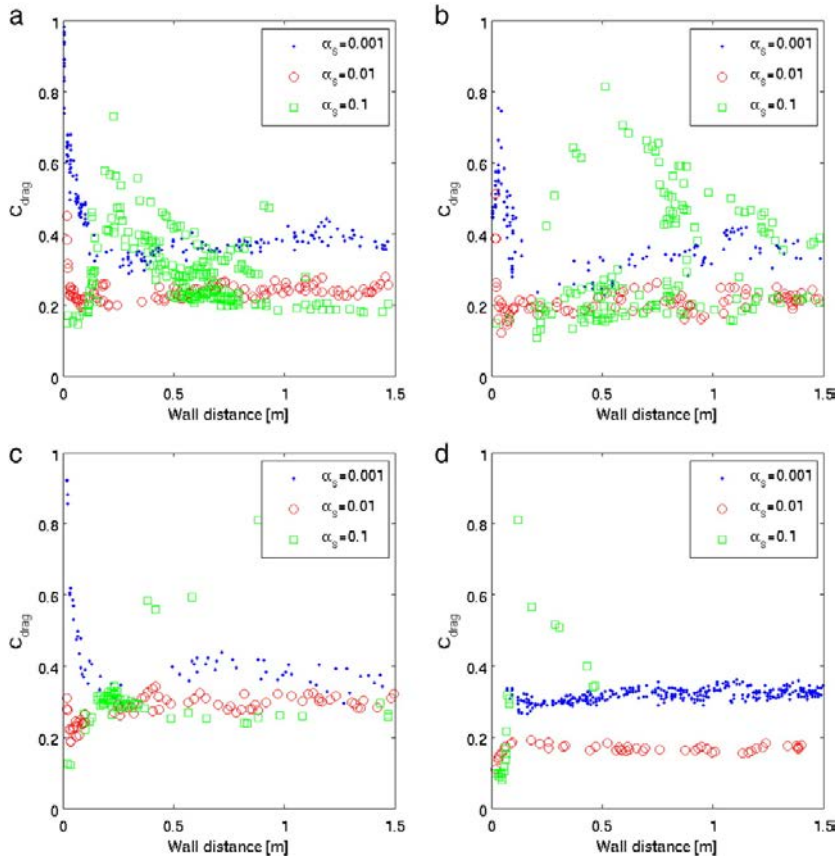

Fig. 8. Effect of the distance to the wall on C_{drag} at different solid volume fractions in Cases 11 (top left), 12 (top right), 13 (bottom left) and 14 (bottom right).

and viscosity varied. Archimedes number, which was also considered as a parameter, gave exactly the same result. Thus the fluid and particle properties need to be separately accounted for.

Fig. 12 shows the effect of varying gas density. It has no clear effect on the drag correction coefficient. According to Fig. 13, solid density has a positive effect on C_{drag}. The effect of gas viscosity is reducing C_{drag} (Fig. 14) indicating that in hot conditions, the drag force deviates stronger than in cold conditions from what it would be if the suspension would be homogeneous. All other properties are the same in the simulations.

Fig. 15 shows that particle size also has a significant effect. Clustering tendency seems to be highest in the case of smallest particles. In large fluidized beds there is typically a big difference in the average particle sizes for the bottom bed and the top of the riser. The largest size in Fig. 15, 0.44 mm, could very well represent the size at bed bottom and the smallest, 0.15 mm, the average size at riser exit. Thus even in a single simulation, a correction function that takes the particle size into account would be needed.

The three phase properties, i.e. solid density, gas viscosity and particle size, which proved to be important for the average drag force, have also a direct effect on the slip velocity. Fig. 10 showed that an increase in slip velocity has a reducing effect on C_{drag}. Thus the possibility that the effect of material properties is due to changes in the slip velocity needs to be considered. This possibility is easily ruled out by studying e.g. the results in Fig. 15. In dilute conditions in the upper part of the riser the slip velocity approaches the terminal velocity of a single particle. Thus we can use the terminal velocities given in Table 1 to indicate the differences in the slip velocity. The terminal velocity increases with particle size and thus C_{drag} in Fig. 15 increases as the slip velocity increases which is opposite to the trend seen in Fig. 10. Thus we can conclude that particle size has an effect separate from that of the slip velocity, which is related to the acceleration of particles while the effect of the particle size is related to changes in the clustering behavior. In a similar way by analyzing Figs. 13 and 14, solid phase density and gas viscosity can be shown to have independent effects.

4. Conclusions

In the present work, parameters affecting the reduction of the average gas–solid drag force in dense gas–solid suspensions due to particle clustering were studied by analyzing time-averaged results from a number of transient simulations carried out in fairly fine meshes. The analysis was limited to Geldart B particles and CFB conditions. The simulations were carried out in 2D, which limits direct quantitative applicability of the results to 2D simulations. Qualitatively, it can be expected that the same parameters that were observed to be important for the average drag force in 2D have also significant effects in 3D geometries. The present results are applicable to time-averaged CFD modeling but not as such to transient coarse mesh simulations. However, since the amount of filtering done by time averaging is similar to the filtering done by a very coarse mesh spacing, the present results indicate that even in coarse mesh closures the parameters that were found to be important in the present work should be considered in development of sub-grid closures.

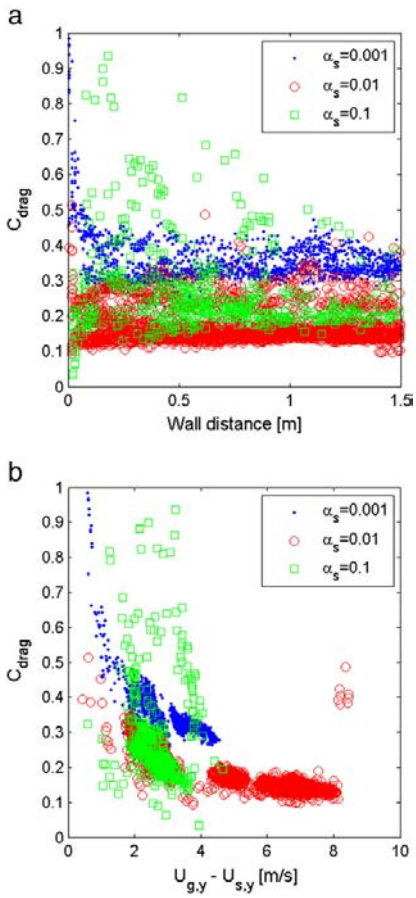

Fig. 9. Summarized data for Cases 9, 10, 11, 12, 13, 14 and 17 at solid volume fractions 0.001, 0.01 and 0.1. a) Drag correction coefficient C_{drag} plotted as a function of the distance to the wall, Δx_{wall}. b) Drag correction coefficient C_{drag} plotted as a function of the slip velocity.

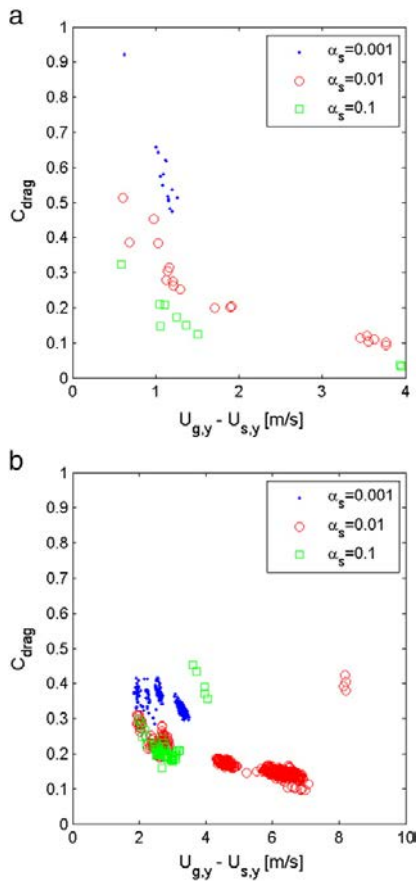

Fig. 10. Summarized data from Cases 9, 10, 11, 12, 13, 14 and 17. Drag correction coefficient C_{drag} plotted as a function of the slip velocity at three different solid volume fractions a) in the wall layer and b) in the central region.

According to the results of the present study, the main parameters that should be accounted for in a relation for the time-averaged gas–solid drag force are the solid volume fraction, distance to the wall, slip velocity, solid phase density, particle size and gas phase laminar viscosity. Thus a closure law should be of the form

$$C_{drag} = f\left(\overline{\alpha_s}, \Delta x_{wall}, \left|U_g - U_s\right|, \rho_s, d_p, \mu_g\right). \quad (4)$$

The distance to the wall has a significant but complicated effect, which was shown to be a result of combined effects with other parameters. Fluidization velocity had an effect on the drag correction but it can probably be at least partly accounted for by including the slip velocity in the model. The present analysis also showed that the effects of material properties cannot easily be lumped together into a single parameter such as a Reynolds number, but they have to be included separately. Within the investigated range, process size and bed mass had no significant effect whereas mesh spacing used in the simulations affected the obtained correction. This implies that drag correction functions can be derived from transient simulations of a small geometry as long as the mesh is fine enough to produce results that are independent of the mesh spacing.

No model was developed in the present study. A wider set of data is necessary for model development to cover possible combined effects of different variables. Only by developing a model we can fully evaluate the extent of the effects of the individual parameters since there can be complicated interactions between them, which weren't studied in the present work.

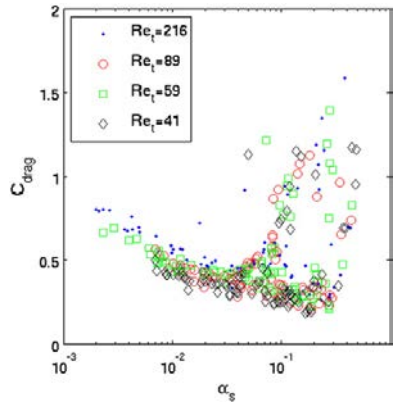

Fig. 11. Effect of Reynolds number (calculated on the basis of particle terminal velocity) on C_{drag} (Cases 8, 5, 6, and 7, respectively, in Table 1). Archimedes numbers for the four cases are 27200, 6900, 3720, and 2180, respectively.

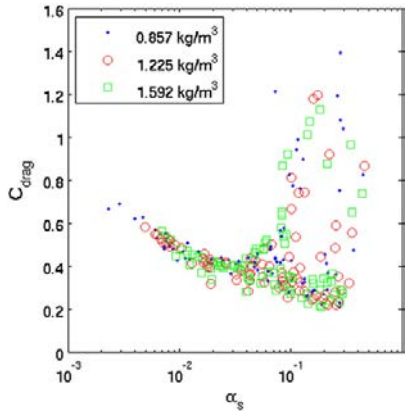

Fig. 12. Effect of gas density on C_{drag} (Cases 6, 3, and 5, respectively, in Table 1).

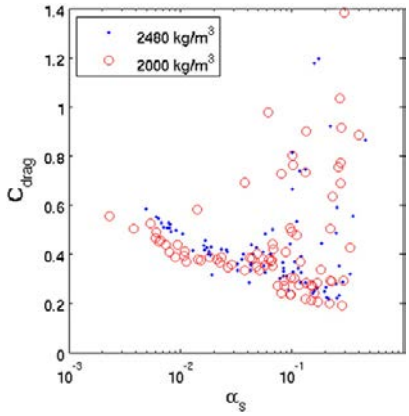

Fig. 13. Effect of solid density on C_{drag} (Cases 3 and 4, respectively, in Table 1).

The models presented in the literature have so far ignored the effects of material properties on the corrections applied on the drag force in coarse mesh and steady state modeling. The present analysis showed that the effects of particle size, solid material density and gas viscosity

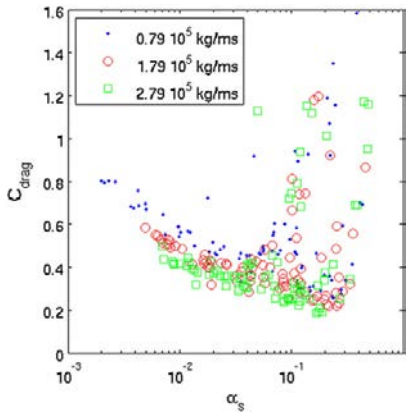

Fig. 14. Effect of gas viscosity on C_{drag} (Cases 8, 3, and 7, respectively, in Table 1).

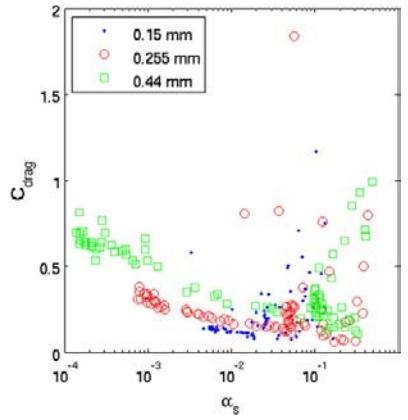

Fig. 15. Effect of particle size on C_{drag} (Cases 16, 14, and 15, respectively, in Table 1).

are significant. Since gas–solid drag strongly affects the vertical distribution of solids in a CFB riser and especially the solid circulation rate, the omission of material property effects from the drag closure significantly reduces the accuracy of the simulations.

Notation

d	diameter
h	height
g	gravitational acceleration
p	pressure
Re	Reynolds number
u	velocity
U	time-averaged velocity
U_0	superficial velocity
v_t	terminal velocity
w	riser width
x	distance
Δx_{mesh}	mesh spacing
Δx_{wall}	distance to wall
K_{qs}	inter-phase momentum transfer coefficient

Greek symbols

α	volume fraction
δ_{qs}	Kronecker delta
μ	viscosity
ρ	density
τ	stress

Subscripts

bot	bottom
k	coordinate k
i	coordinate i
g	gas
p	particle
q	phase q
s	solid
t	related to terminal velocity

Superscripts

M	turbulent
$*$	calculated from time-averaged values

Acknowledgment

The authors gratefully acknowledge the financial support of Tekes, VTT Technical Research Centre of Finland, Etelä-Savon Energia Oy, Fortum, Metso Power Oy and Numerola Oy, and the support from Saarijärven Kaukolämpö Oy.

References

[1] S. Benyahia, S. Sundaresan, Do we need sub-grid scale corrections for both continuum and discrete gas–particle flow models? Powder Technol. 220 (2012) 2–6.
[2] V. Taivassalo, S. Kallio, J. Peltola, On time-averaged CFD modeling of circulating fluidized beds, Int. J. Nonlinear Sci. Numer. Simul. 13 (2012) 363–373.
[3] Zh.X. Zeng, L.X. Zhou, A two-scale second-order moment particle turbulence model and simulation of dense gas–particle flows in a riser, Powder Technol. 162 (2006) 27–32.
[4] S. Kallio, V. Taivassalo, T. Hyppänen, Towards time-averaged CFD modelling of circulating fluidized beds, 9th Int. Conf. on Circulating Fluidized Beds, Hamburg, 2008.
[5] S. Kallio, V. Poikolainen, T. Hyppänen, Mathematical modeling of multiphase flow in a circulating fluidized bed, Report 96-4, Heat Eng. Lab.Åbo Akademi University, Turku, Finland, 1996.
[6] J.M. Matsen, Mechanisms of choking and entrainment, Powder Technol. 32 (1982) 21–33.
[7] S. Ergun, Fluid flow through packed columns, Chem. Eng. Prog. 48 (1952) 89.
[8] K. Agrawal, P.N. Loezos, M. Syamlal, S. Sundaresan, The role of mesoscale structures in rapid gas–solid flows, J. Fluid Mech. 445 (2001) 151–185.
[9] A.T. Andrews, P.N. Loezos, S. Sundaresan, Coarse-grid simulation of gas–particle flows in vertical risers, Ind. Eng. Chem. Res. (2005) 6022–6037.
[10] Y. Igci, S. Sundaresan, S. Pannala, T. O'brien, R.W. Breault, Coarse-graining of two-fluid models for fluidized gas–particle suspensions, 5th Int. Conf. on CFD in the Process Industries, CSIRO, Melbourne, Australia, 2006.
[11] Y. Igci, A.T. Andrews, S. Sundaresan, S. Pannala, T. O'Brien, Filtered two-fluid models for fluidized gas–particle suspensions, AIChE J 54 (2008) 1431–1448.
[12] Y. Igci, S. Sundaresan, Verification of filtered two-fluid models for gas–particle flows in risers, AIChE J 57 (2011) 2691–2707.
[13] Y. Igci, S. Pannala, S. Benyahia, S. Sundaresan, Validation studies on filtered model equations for gas–particle flows in risers, Ind. Eng. Chem. Res. 51 (2012) 2094–2103.
[14] C.C. Milioli, F.E. Milioli, W. Holloway, K. Agrawal, S. Sundaresan, Filtered two-fluid models of fluidized gas–particle flows: new constitutive equations, 59 (2013) 3265–3275.
[15] S. Shah, J. Ritvanen, T. Hyppänen, S. Kallio, Wall effects on space averaged two-fluid model equations for simulations of gas–solid flows in risers, Chem. Eng. Sci. 89 (2013) 206–215.
[16] D.Z. Zhang, W.B. VanderHeyden, High-resolution three-dimensional numerical simulation of a circulating fluidized bed, Powder Technol. 116 (2001) 133–141.
[17] D.Z. Zhang, W.B. VanderHeyden, The effects of mesoscale structures on the macroscopic momentum equations for two-phase flows, Int. J. Multiphase Flow 28 (2002) 805–822.
[18] J. De Wilde, The generalized added mass revised, Phys. Fluids 19 (2007) 058103.
[19] J. De Wilde, G.J. Heynderickx, G.B. Martin, Filtered gas–solid momentum transfer models and their application to 3D steady-state riser simulations, Chem. Eng. Sci. 62 (2007) 5451–5457.
[20] W. Wang, J. Li, Simulation of gas–solid two-phase flow by a multi-scale CFD approach—extension of the EMMS model to the sub-grid level, Chem. Eng. Sci. 62 (2007) 208–231.
[21] X. Wang, F. Jiang, J. Lei, J. Wang, S. Wang, X. Xu, Y. Xiao, A revised drag force model and the application for the gas–solid flow in the high-density circulating fluidized bed, Appl. Therm. Eng. 31 (2011) 2254–2261.
[22] ANSYS Inc., ANSYS FLUENT Theory Guide. Release 14.0, Canonsburg, 2011.
[23] D. Gidaspow, Multiphase Flow and Fluidization — Continuum and Kinetic Theory Descriptions, Academic Press, 1994.
[24] C. Wen, Y. Yu, Mechanics of fluidization, Chem. Eng. Prog. Symp. Ser. 62 (1966) 100–111.
[25] S. Kallio, M. Guldén, A. Hermanson, Experimental study and CFD simulation of a 2D circulating fluidized bed, The 20th Int. Conf. on Fluidized bed combustion. May 18–20, Xi'an, China, 2009.
[26] M. Syamlal, W. Rogers, T.J. O'Brien, MFIX documentation: volume 1, theory guide, DOE/METC-9411004, NTIS/DE9400087, National Technical Information Service, Springfield, VA, 1993.
[27] C.K.K. Lun, S.B. Savage, D.J. Jeffrey, N. Chepurniy, Kinetic theories for granular flow: inelastic particles in couette flow and slightly inelastic particles in a general flow field, J. Fluid Mech. 140 (1984) 223–256.
[28] D.G. Schaeffer, Instability in the evolution equations describing incompressible granular flow, J. Differ. Equ. 66 (1987) 19–50.
[29] S. Ogawa, A. Umemura, N. Oshima, On the equations of fully fluidized granular materials, J. Appl. Math. Phys. (ZAMP) 31 (1980) 483–493.
[30] T. Niemi, J. Peltola, S. Kallio, Time averaged modeling of BFBs: analysis of the terms in the momentum equations, Proceedings Fluidization XIV Conference, May 2013, Noordwijkerhout, The Netherlands, 2013, pp. 559–566.
[31] J. Leboreiro, G.G. Joseph, C.M. Hrenya, Revisiting the standard drag law for bubbling, gas-fluidized beds, Powder Technol. 183 (2008) 385–400.